Article

Fatigue Limit Improvement and Rendering Surface Defects Harmless by Shot Peening for Carburized Steel

Toshiya Tsuji [1], Masashi Fujino [2] and Koji Takahashi [3,*]

1   Process Development Team, Development Group, SINTOKOGIO, Ltd., 180-1 Komaki, Ohgi-cho, Toyokawa City 441-1205, Japan
2   Graduate School of Engineering, Yokohama National University, 79-5 Tokiwadai, Hodogaya, Yokohama 240-8501, Japan
3   Faculty of Engineering, Yokohama National University, 79-5 Tokiwadai, Hodogaya, Yokohama 240-8501, Japan
*   Correspondence: takahashi-koji-ph@ynu.ac.jp

Abstract: Remanufacturing has become popular as a system for reducing CO_2 emissions caused by the life cycle of products. Therefore, producing more components via remanufacturing is important. Shot peening can be used to render surface defects harmless owing to the compressive residual stress effects. This study investigated the effects of shot peening as a means of remanufacturing gears. In this study, carburized steel specimens containing artificial defects were used to investigate the effects of shot peening on the fatigue strength; the defect size was rendered harmless by shot peening. Shot peening was conducted after inducing semicircular slits with depths of a = 0.15, 0.20, and 0.30 mm. Subsequently, plane bending fatigue tests were carried out. A maximum compressive residual stress of 1400 MPa was induced after shot peening. The fatigue limit of the smooth specimen increased by approximately 31% after shot peening. A semicircular slit of at least 0.20 mm deep could be rendered harmless by shot peening (SP). The defect size reduced by SP was evaluated on the basis of fracture mechanics. The estimated results are consistent with the experimental results. On the basis of the results, the feasibility of shot peening as a remanufacturing method for gears is discussed.

Keywords: shot peening; carburized steel; remanufacturing; residual stress; fatigue

1. Introduction

Remanufacturing is a system that reuses the equivalent used parts to manufacture new parts [1]. Remanufacturing gears can reduce CO_2 emissions through waste management and recycling [2]. This is because manufacturing gears cause large amounts of CO_2 due to heated production processes, such as hot forging and heat treatment. Furthermore, the reduction in CO_2 emissions increases upon increasing the number of remanufactured gears. Many researchers have reported that gears fail from surface cracks by bending fatigue at the tooth root or micro pits on the tooth flank [3]. It is difficult to apply remanufacturing to used gears because of surface defects that contribute to fatigue failure. For this reason, a technology that can render surface defects harmless is required to increase the number of gears processed with remanufacturing. Several researchers have reported that shot peening [4,5] and alternative peening [6,7] can render surface defects harmless due to the effect of compressive residual stress. Takahashi et al. investigated the bending fatigue strengths of spring steel that contained a semicircular surface slit and reported that a semicircular slit at least 0.2 mm deep could be rendered harmless by shot peening [4]. They reported a prediction method for the defect size that can be rendered harmless by shot peening, considering the influence of the compressive residual stress distribution [4]. Kubota et al. investigated the fatigue properties of spring steel specimens subjected to double- and triple-shot peening. They found that the fatigue limits of the specimens with 0.25 mm deep artificial corrosion pits were remarkably improved by triple-shot peening [5]. Laser peening is an alternative peening technology that can induce compressive residual stresses.

The compressive residual stress layer induced by laser peening is deeper than that achieved by shot peening [8,9]. The effect of laser peening on the fatigue strength of specimens with surface defects has been evaluated in aluminum alloys [6] and maraging steels [7]. It has been reported that larger surface defects can be rendered harmless in specimens subjected to laser peening compared to those subjected to shot peening [6]. Cavitation peening can induce compressive residual stress by generating plastic deformation owing to shock waves when cavitation bubbles collapse [10]. It has been reported that cavitation peening can render surface defects of at least 0.2 mm deep harmless in terms of fatigue strength [11].

According to the findings of these studies, peening technology can be utilized to remanufacture carburized steel used in transmission gears. However, laser peening and cavitation peening are difficult to apply to parts with complex geometries such as gears. Therefore, shot peening is appropriate peening technology for transmission gears. In general, the surface Vickers hardness (HV) of carburized steel is extremely hard, more than 700 HV. However, most previous reports focused on metals with hardness less than 500 HV [4–7]. The effects of shot peening on the defect size rendered harmless by shot peening have not been investigated in carburized steel. As the hardness of the material increases, the reduction in fatigue strength resulting from surface defects also increases. Therefore, it is challenging to render the surface defects harmless by shot peening in carburized steels. Moreover, the applicability of the prediction method of the defect size rendered harmless by shot peening [4] has not been investigated for carburized steel.

In this study, we conducted plane bending fatigue tests for carburized steel that was shot-peened after inducing a semicircular slit. The defect size rendered harmless by shot peening was estimated on the basis of the fracture mechanics. These results suggest that shot peening is a useful method for remanufacturing gears.

2. Experimental Method

2.1. Material and Specimen

A hot-rolled round bar of chromium molybdenum steel (JIS SCM420H) with a diameter of 100 mm was used. This steel is widely used in transmission gears. Table 1 lists the chemical composition of this material. Figure 1 shows the shapes and dimensions of the specimens. Figure 2 shows the flowchart of the specimen manufacturing process. The specimens were taken such that the longitudinal direction was perpendicular to the rolling direction of the round bars. Vacuum normalizing was conducted before machining to homogenize the microstructure. The material was machined into the shape of a specimen.

Table 1. Chemical composition of JIS SCM420H (wt.%).

C	Si	Mn	P	S	Cu	Ni	Cr	Mo
0.23	0.31	0.81	0.013	0.017	0.07	0.05	1.21	0.23
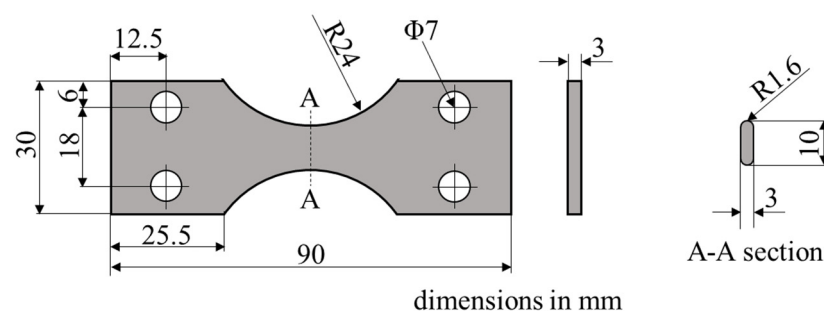
dimensions in mm

Figure 1. Shape and dimensions of the specimen (mm).

```
┌─────────────────────────────────────────────────────┐
│           Vacuum Normalizing (1198K, 3600s)           │
└─────────────────────────────────────────────────────┘
                          ↓
┌─────────────────────────────────────────────────────┐
│                     Machining                          │
└─────────────────────────────────────────────────────┘
                          ↓
┌─────────────────────────────────────────────────────┐
│ Vacuum Carburizing(1203K, 7560s) Quenching (1123K,    │
│          3600s) - Tempering(433K, 7200s)              │
└─────────────────────────────────────────────────────┘
```

Figure flow:
- Vacuum Normalizing (1198K, 3600s) → Machining → Vacuum Carburizing(1203K, 7560s) Quenching (1123K, 3600s) - Tempering(433K, 7200s)
  - → Non-SP
  - → Shot Peening → SP
  - → Slit
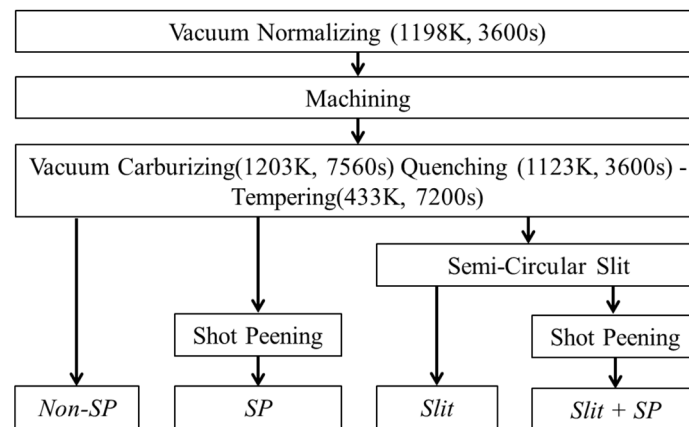 - → Semi-Circular Slit → Shot Peening → Slit + SP

Figure 2. Flow chart of the specimen manufacturing process.

Vacuum carburizing, quenching, and tempering, which are used in transmission gears as surface-enhancement treatments, were employed. Figure 3 shows the microstructure observation results of the cross-section of the specimen after vacuum carburizing. The polished surface was etched with a 5% nital solution. The structure near the surface of this carburized steel consisted of martensite and retained austenite. There was no incomplete quenching structure (bainite) or intergranular oxide layer. The reason for the presence of retained austenite is that the carburizing process increased the carbon concentration near the surface and lowered the martensitic transformation start temperature (Ms point) and martensitic transformation finish temperature (Mf point) [12].
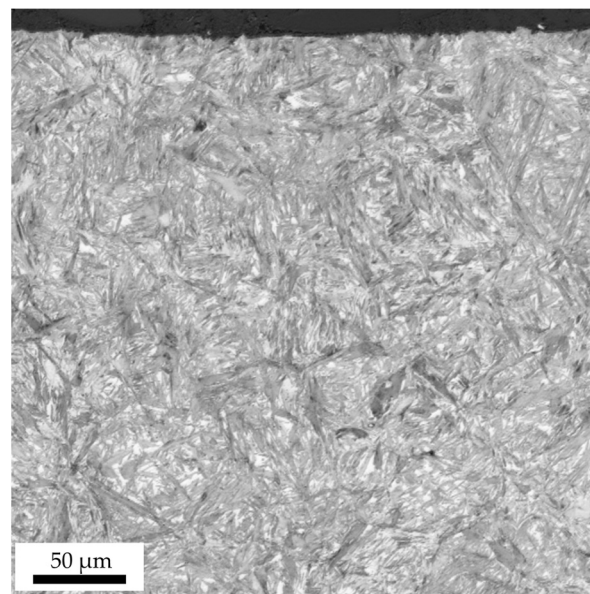

Figure 3. Microstructure after vacuum carburizing quenching and tempering near the surface.

As an artificial surface defect, a semicircular slit was induced on the surface of the specimen by electric discharge machining to simulate an initial crack-like surface defect. Figure 4 depicts the shape and dimensions of the surface slit. The semicircular slit depths were 0.15, 0.20, and 0.30 mm.
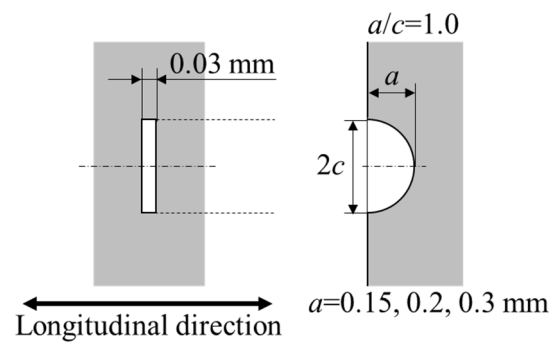
Figure 4. Shapes and dimensions of the artificial defect.

Slit + SP specimens were subjected to shot peening after introducing a slit, as shown in Figure 2. Table 2 shows the condition of the shot peening. The shot peening conditions applied in this study were typical conditions for carburized gears [13].

Table 2. Shot peening condition.

Media	Conditioned Cut Wire Of Steel
Media diameter	0.60 mm
Media hardness	700 HV
Projection method	Direct air pressure type
Air pressure	0.30 MPa
Coverage	300%
Arc height	0.518 mmA

2.2. Measurement of the Surface Roughness, Vickers Hardness, and Residual Stress

The surface roughness, hardness distribution, and residual distribution were measured for each specimen type.

A stylus-type surface roughness tester (SURFCOM 1400D, Tokyo Seimitsu Co., Ltd., Tokyo, Japan) was used to measure surface roughness. The cutoff value was 0.8 mm, and the measurement length was 4.0 mm. The average surface roughness *Ra* and maximum height roughness *Rz* were measured in this study. Measurements were obtained for three specimens of each specimen type.

The Vickers hardness distribution from the surface to depth was measured using a micro-Vickers hardness tester (HVM-113, Mitutoyo Corporation, Kawasaki, Japan). Measurements were collected three times at each depth with a measurement load of 0.98 N and a load holding time of 10 s.

Residual stress was measured using an X-ray residual stress measurement device (μX-360S, PLUSETEC Industrial Co., Ltd., Nakagawa, Japan). The cosα method was used for analysis. The characteristic X-ray was Cr Kα, and the diffraction plane was α-Fe (211). The residual stress distribution in the depth direction was obtained by alternately measuring the surface residual stress and removing the surface layer via electropolishing. Because stress redistribution occurred after the removal of the surface layer, a stress correction calculation was performed for each measurement result [14]. To confirm the residual stress relaxation by fatigue testing, the residual stress of the specimens was measured before and after fatigue testing. For the measurement of residual stress after fatigue testing, runout specimens at the fatigue limit were used.

2.3. Fatigue Test Method

The fatigue test was conducted using a plane bending fatigue test machine (PBF-60Xa, Tokyo Koki Co. Ltd., Sagamihara, Japan) under a stress ratio $R = -1$ and a test frequency of 20 Hz. The fatigue tests were performed at room temperature in an air atmosphere. The number of runouts was 1.0×10^7 cycles. The fatigue limit was defined as the maximum

stress amplitude at which the specimen could withstand 10^7 stress cycles. The fracture surface was observed using a scanning electron microscope (VE-8800, Keyence Ltd., Osaka, Japan)) to investigate the fracture origin.

3. Results

3.1. Surface Roughness

Table 3 shows the measurement results of surface roughness. The *Rz* of the SP specimen was approximately twofold higher than that of the non-SP specimen. This is because the shot peening process generated dimples on the surface due to plastic deformation by impacting spherical media. This surface roughness value of SP specimen was sufficiently small compared to the depth of the slit introduced into the specimen.

Table 3. Surface roughness values.

Symbol	*Ra* (μm)	*Rz* (μm)
Non-SP	0.194	1.368
SP	0.470	2.633

3.2. Hardness Distribution

Figure 5 shows the distribution of the Vickers hardness. The surface hardness of the non-SP specimen was approximately 730 HV. The hardness near the surface was much higher than the base metal hardness of this material (approximately 400–500 HV). This increase in hardness was attributed to the formation of a large amount of martensite due to carburizing and quenching. The effective case depth was approximately 0.9 mm. The ratio of retained austenite on the surface of the non-SP specimen was approximately 13.1 vol.%. The ratio of retained austenite was defined as the volume ratio of austenite to martensite, as measured by X-ray diffraction. The hardness of the SP specimens increased to a depth of 0.2 mm by approximately 100 HV compared to the non-SP specimen. The volume of the retained austenite on the surface of the SP specimen was approximately 1.3 vol.%. The retained austenite content of the SP specimen was lower than that of the non-SP specimen. Tsuji et al. conducted shot peening on steels with different retained austenite [15]. As a result, hardness improvement by shot peening was obtained even in steels with low amounts of retained austenite. Therefore, the increase in hardness due to shot peening was caused by both work hardening and deformation-induced martensite. The hardness of the non-SP specimen at depths deeper than 1.0 mm was higher than that of the SP specimen. This was assumed to be due to the variation in the amount of carbon penetration by the carburizing treatment of the specimen.
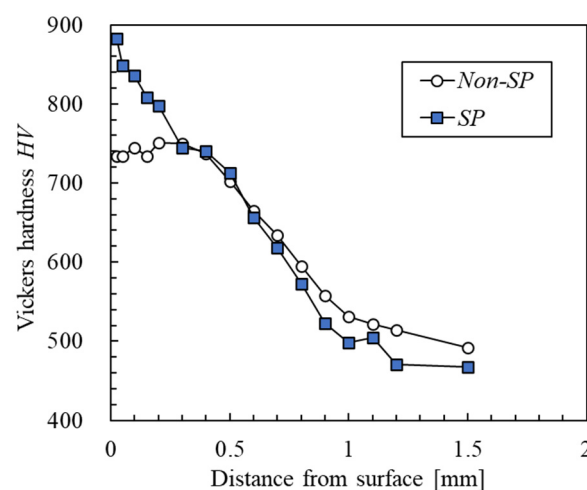

Figure 5. Distribution of Vickers hardness.

3.3. Residual Stress Distribution

Figure 6 shows the residual stress distribution before and after the fatigue test. Before the fatigue test, the surface compressive residual stress was approximately 800 MPa. The maximum compressive residual stress of the SP specimen was approximately 1400 MPa, measured at the depth of 0.05 mm. This was characteristic of the residual stresses introduced by shot peening, whereby a maximum compressive residual stress was produced at the inside rather than on the surface. The crossing point where the residual stress changed from compression to the tension was approximately 0.3 mm. After the fatigue test, the residual stresses in the non-SP and SP specimens did not decrease. When compressive stress was applied to steel with residual stress, compressive yielding occurred, and the compressive residual stress decreased [16]. However, the carburized steel used in this study had a high yield stress due to its high surface hardness. Therefore, a decrease in compressive residual stress did not occur.
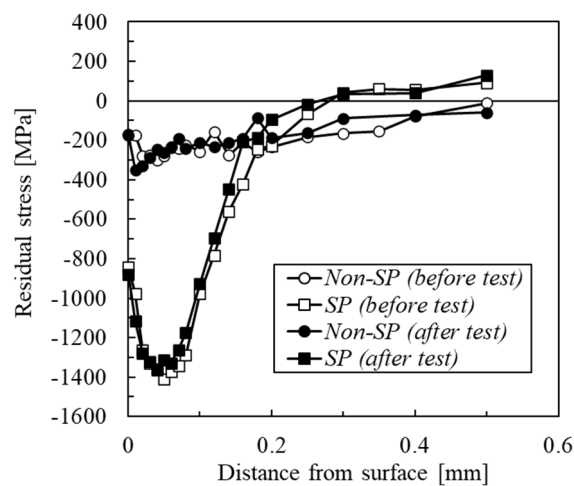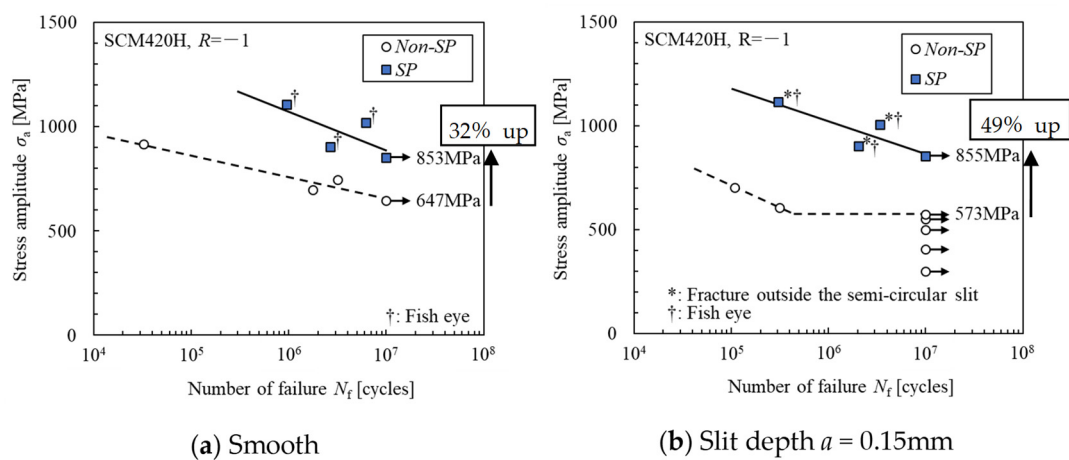

Figure 6. Distribution of residual stress.

3.4. Fatigue Test Results

Figure 7 shows the fatigue test results of each specimen type. An asterisk denotes that the specimen fractured outside the slit. A cross denotes the specimen fractured from inclusion and resulted in the fisheye fracture mode.

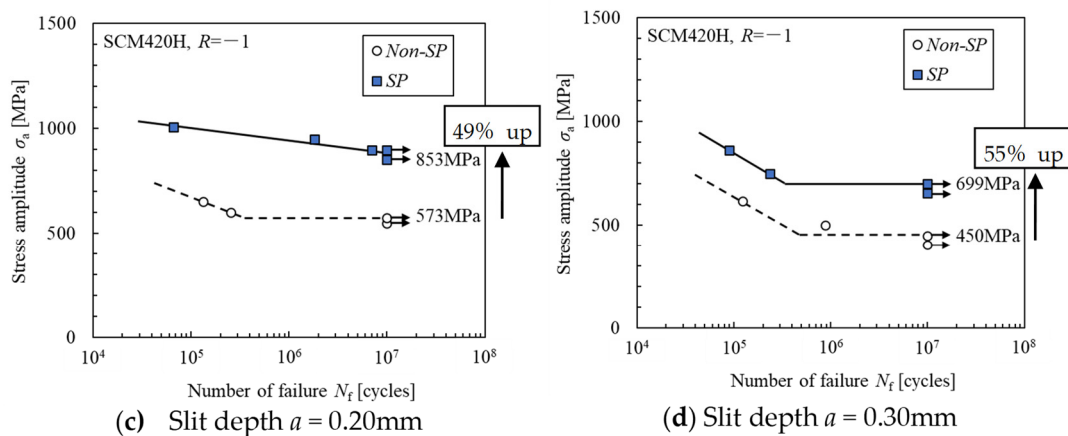(**a**) Smooth

(**b**) Slit depth *a* = 0.15mm

Figure 7. *Cont.*

Figure 7. Fatigue test results. (**a**) Smooth, (**b**) Slit depth *a* = 0.15 mm, (**c**) Slit depth *a* = 0.20 mm, (**d**) Slit depth *a* = 0.30 mm.

In the smooth specimens shown in Figure 7a, the fatigue limit of the SP specimen was 32% higher than that of the non-SP specimen owing to the increased hardness and compressive residual stress due to shot peening. The fatigue life of the SP specimen was also significantly extended. As shown in Figure 7b–d, the fatigue limit of the slit specimens decreased compared to that of the smooth specimen by introducing the slit.

In the case of the slit depths of 0.15 mm and 0.20 mm shown in Figure 7b,c, the fatigue limit of the SP specimen was 49% higher than that of the non-SP specimen (573 MPa). Furthermore, these fatigue limits were equivalent to those of the smooth specimens with SP.

For the slit depth of 0.30 mm shown in Figure 7d, the fatigue limit of the SP specimen was 699 MPa, which was lower than that of the smooth specimen with SP. The fatigue limit of the SP specimen was 55% higher than that of the non-SP specimen, even though the slit depth of 0.3 mm was deeper than the crossing point of the compressive residual stress. This is presumably because the integrated value of the compressive residual stress from the surface to the tip of the slit contributed significantly to the suppression of crack propagation.

Figure 8 shows the fracture surface of the smooth specimen. In the case of smooth specimens without an artificial defect. The crack initiation point of the non-SP specimen was on the surface under all conditions (see Figure 8a). On the other hand, the SP specimen exhibited a fisheye fracture mode. The fisheye occurred from the inclusion at the depth of about 400 μm from the surface (see Figure 8b). Thus, the increase in surface roughness by shot peening mentioned in Section 3.1 did not affect the fatigue limit, because the crack initiation point of the SP specimen was not on the surface.
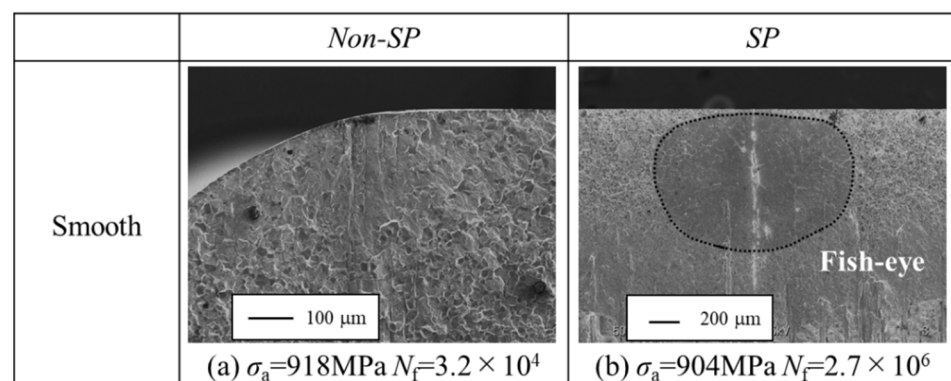

Figure 8. Fracture surface observation results of smooth specimens.

Elongated nonmetallic inclusion was observed at the center of the fish eye (see Figure 8b). Energy-dispersive X-ray spectroscopy (EDX) revealed that the composition of the inclusion

was MnS. Furuya performed gigacycle fatigue tests on high-strength steel (JIS-SCM440), which was intentionally integrated with high MnS content [17]. It was suggested that largely elongated MnS reduced the fatigue strength.

Figure 9 shows the fatigue fracture surface observation results of each slit specimen. Figure 9a shows the fracture surface of the 0.15 mm slit specimen fractured from the slit. On the other hand, slit + SP specimens with a slit depth of a = 0.15 mm, shown in Figure 9b, failed outside the slit. This fracture mode was a fisheye-type fracture. The elongated MnS was observed at fracture origin. The 0.20 mm and 0.30 mm non-SP specimens fractured from the slit, as shown in Figure 9c,e. Slit + SP specimens with slit depths of 0.20 and 0.30 mm shown in Figure 9d,f failed from the slit. The shape of the slit in the slit + SP specimen showed some deformation only near the surface as shown in Figure 9d,f. However, there is no change in the slit shape at the sub-surface. Thus, the effect of the deformation of the slit due to SP on the fatigue strength was small.
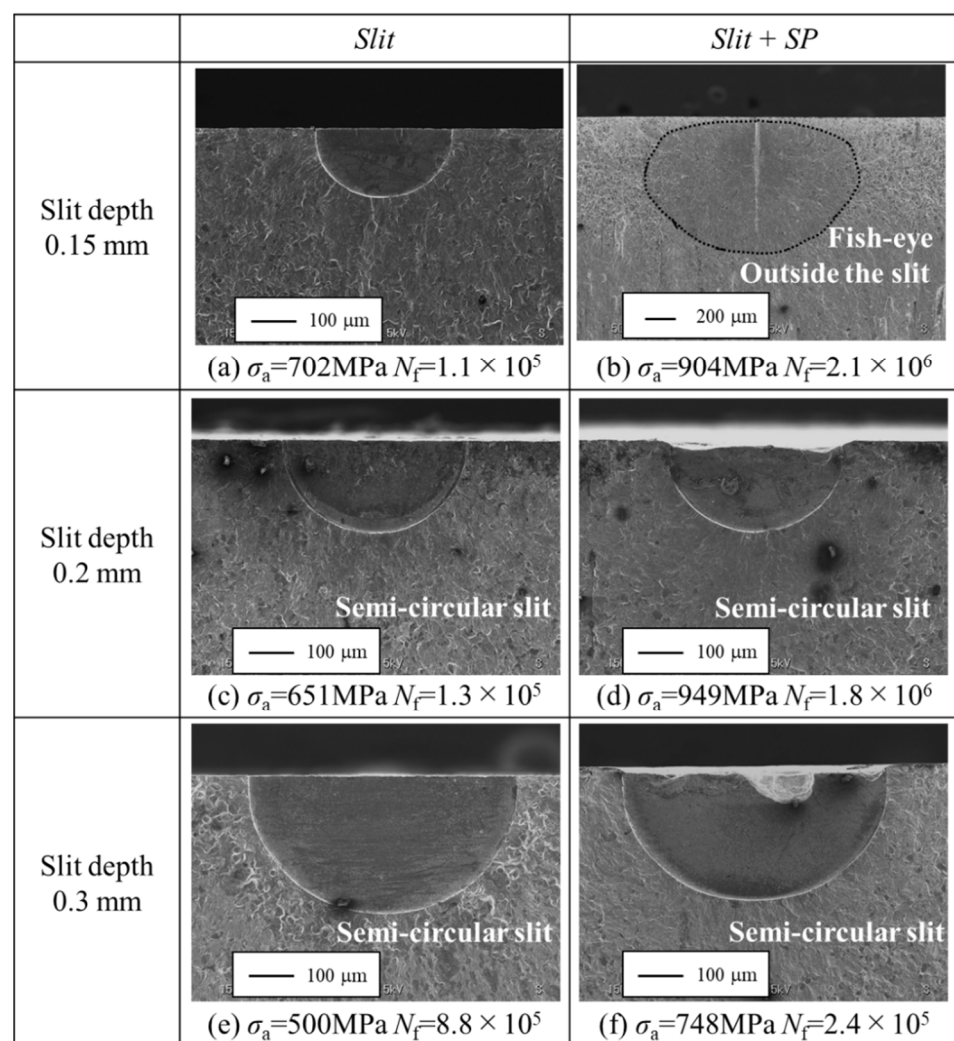

	Slit	*Slit + SP*
Slit depth 0.15 mm	(a) σ_a=702MPa N_f=1.1 × 10^5	(b) σ_a=904MPa N_f=2.1 × 10^6
Slit depth 0.2 mm	(c) σ_a=651MPa N_f=1.3 × 10^5	(d) σ_a=949MPa N_f=1.8 × 10^6
Slit depth 0.3 mm	(e) σ_a=500MPa N_f=8.8 × 10^5	(f) σ_a=748MPa N_f=2.4 × 10^5

Figure 9. Fracture surface observation results of slit specimens.

Figure 10 shows the relationship between slit depth and stress amplitude. The solid and open marks indicate the failed and runout specimens, respectively. In this study, we determined that the slit was rendered harmless if the fatigue test results satisfied either of the following two conditions, similar to previous studies [6]:

(a) The fatigue limit of the slit + SP specimen increased to more than 95% of that of the SP specimen.

(b) More than half the specimens fractured outside the slit.
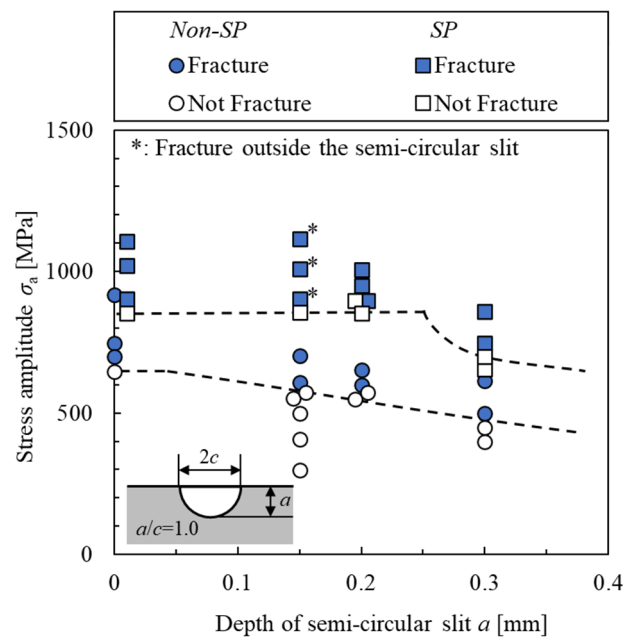
Figure 10. Relationship between stress amplitude and slit depth.

The fatigue limit of the non-SP specimen decreased with increasing slit depth. On the other hand, the fatigue limit of the slit + SP with slit depths a = 0.15 mm and 0.20 mm increased to 49% of the fatigue limit of the slit specimen, as shown in Figure 10. Therefore, a semicircular slit with a depth of at least 0.20 mm could be rendered harmless by shot peening.

4. Discussion

4.1. Evaluation of Defect Size Rendered Harmless by Shot Peening

Takahashi et al. reported that the defect size rendered harmless by SP (a_{max}) can be evaluated on the basis of fracture mechanics, assuming that a surface defect is equivalent to a surface crack [4]. The positive value of the stress intensity factor range (ΔK_T) was calculated using Equation (1) because ΔK_T affects fatigue crack propagation.

$$\Delta K_T = K_{max} + K_R, \tag{1}$$

where K_{max} is the stress intensity factor at the maximum applied stress calculated using the Newman–Raju equation [18]. The fatigue limit of the SP specimen (σ_{max} = 853 MPa) was considered as the maximum applied stress when calculating K_{max}. K_R is the stress intensity factor of the residual stress induced by shot peening. The quadratic equation of API RP579 was employed to calculate the stress intensity factor of the residual stress field [19]. The stress intensity factor of a semicircular crack in a flat plate was calculated using Equation (2).

$$K_R = \left[G_0\sigma_0 + G_1\sigma_1\left(\frac{a}{t}\right) + G_2\sigma_2\left(\frac{a}{t}\right)^2 + G_2\sigma_2\left(\frac{a}{t}\right)^3 + G_3\sigma_3\left(\frac{a}{t}\right)^3 \right] \sqrt{\frac{\pi a}{Q}} f_w, \tag{2}$$

$$Q = 1.0 + 1.464\left(\frac{a}{c}\right)^{1.65}, \quad f_w = \left\{ sec\left(\frac{\pi c}{2W}\sqrt{\frac{a}{t}}\right) \right\}^{0.5},$$

where G_0 to G_4 are the shape correction coefficients of the stress intensity factor, which is defined in API RP579, a is the depth and c is the half surface crack length of the semicircular crack, W is the width of the specimen at the minimum cross-section, t is the thickness of

the specimen, and σ_0 to σ_4 are coefficients obtained by approximating using the quartic equation for the residual stress distribution using Equation (3).

$$\sigma_R(x) = \sigma_0 + \sigma_1\left(\frac{x}{t}\right) + \sigma_2\left(\frac{x}{t}\right)^2 + \sigma_3\left(\frac{x}{t}\right)^3 + \sigma_4\left(\frac{x}{t}\right)^4, \tag{3}$$

where x denotes the distance from the surface. In this study, the residual stress distribution of the shot-peened specimens after the fatigue test was considered when calculating K_R.

Figure 11 depicts the relationship between ΔK_T of the semicircular slit and the depth of the SP specimen. $\Delta K_{T, A}$ and $\Delta K_{T, c}$ are ΔK_T at the deepest point and the surface of a semicircular slit, respectively. The value of ΔK_{th} depends on the crack size because the crack type targeted in this study is the so-called small crack. Many equations regarding the dependence of crack length were proposed in the literature [20,21]. Equation (4) reported by Ando et al. was employed to calculate ΔK_{th} in this study [22].

$$\Delta K_{th} = 2\alpha\sigma_w\sqrt{\frac{a}{\pi}}\cos^{-1}\left[\left\{\frac{\pi}{8\alpha^2 a}\left(\frac{\Delta K(L)_{th}}{\sigma_w}\right)^2 + 1\right\}^{-1}\right], \tag{4}$$

where $\Delta K(L)_{th}$ is the threshold stress intensity factor range for a large crack, σ_w is the fatigue limit of a non-SP specimen, and α is the shape correction coefficient of the crack, which was calculated using the Newman–Raju equation [18]. A semicircular slit with $a = 0.3$ mm was regarded as a large crack. The corresponding $\Delta K(L)_{th}$ value was calculated using Equation (5).

$$\Delta K(L)_{th} = \alpha\sigma_{w,slit0.3}\sqrt{\pi a}, \tag{5}$$

where $\sigma_{w,slit0.3}$ is the fatigue limit of the slit specimen with a slit depth $a = 0.30$ mm. Substituting $\sigma_{w,slit0.3} = 450$ MPa into Equation (5), $\Delta K(L)_{th}$ was calculated as 7.94 MPa·m$^{1/2}$.
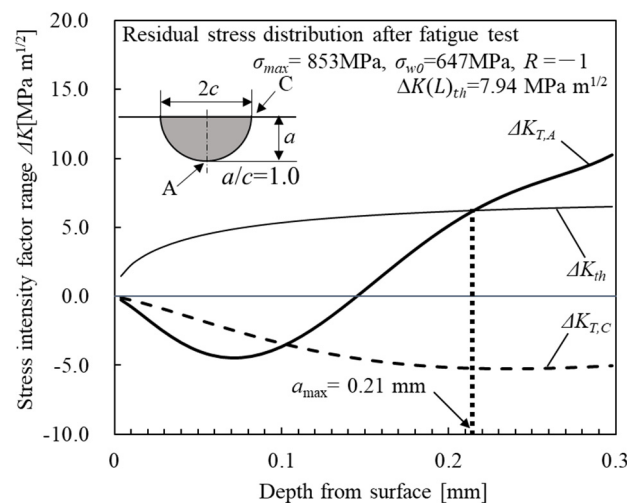

Figure 11. Relationship between stress intensity factor range and depth from the surface.

Assuming that the semicircular slit is equivalent to a semicircular crack, it is possible to evaluate whether the semicircular slit can be rendered harmless, according to the relationship between ΔK_T and ΔK_{th}. If ΔK_T is less than ΔK_{th}, the slit is considered harmless. Therefore, a_{max} was estimated from the intersection between ΔK_T and ΔK_{th} [4]. The a_{max} of the SP specimen was 0.21 mm, as shown in Figure 11. This result is consistent with the experimental result that a semicircular slit with a depth of at least 0.2 mm can be rendered harmless by SP, whereas a surface slit with a depth of 0.3 mm cannot. Therefore, a_{max} of shot-peened carburized steel can be evaluated by employing this method.

4.2. Application of Shot Peening to the Remanufacturing Process

On the basis of the experimental and analytical results obtained in this study, we propose a remanufacturing process for carburized steel using shot peening, as shown in Figure 12. First, the cracks in the used parts were inspected by nondestructive testing, such as eddy current tests and ultrasonic testing. If the detected crack size is less than a_{max}, shot peening is effective in rendering the defect harmless. However, the shot peening condition considered in this study is not effective for remanufacturing if the crack size of the used parts is larger than 0.2 mm. Note that a_{max} is strongly dependent on the shot peening conditions. A future challenge for this process is to increase the a_{max}.
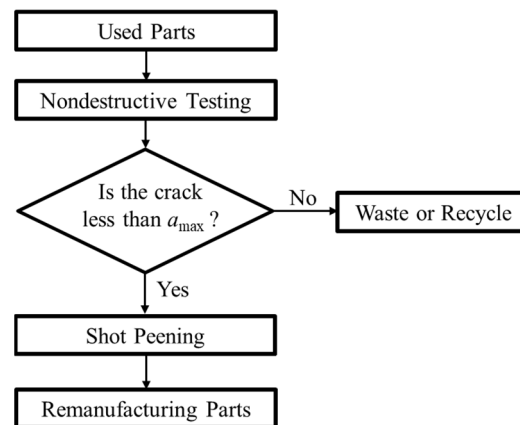

Figure 12. Flowchart of remanufacturing process with shot peening.

5. Conclusions

1. The hardness of carburized steel increased to 100 HV owing to deformation-induced martensite and work hardening caused by shot peening. The maximum compressive residual stress was 1400 MPa, and the crossing point was approximately 300 μm in the shot-peened specimen. A decrease in compressive residual stress after the fatigue test did not occur. This was due to the extremely high surface hardness of carburized steel.

2. The fatigue limit of the smooth specimen increased by approximately 31% after the shot peening. This was attributed to the increase in surface hardness due to shot peening and the fact that the compressive residual stresses were not reduced during the fatigue tests.

3. The fatigue limit of the slit + SP with slit depths of 0.15 and 0.20 mm increased by 49% compared to the fatigue limit of the non-SP specimen. Furthermore, these fatigue limits were equivalent to those of the smooth specimens with SP. Therefore, a semicircular slit at least 0.20 mm deep could be rendered harmless by shot peening. Therefore, the effectiveness of shot peening in rendering surface defects harmless was clarified for carburized steels with Vickers hardness over 700 HV.

4. The defect size rendered harmless by SP (a_{max}) was evaluated on the basis of the fracture mechanics. The estimated a_{max} was 0.21 mm. This evaluation result was consistent with the experimental results. Therefore, the defect size rendered harmless by shot peening can be successfully predicted for shot-peened carburized steel with a surface hardness larger than 700 HV as a function of the fracture mechanics.

Conflicts of Interest: The authors declare no conflict of interest.

References

1.   Kanazawa, T.; Matsumoto, M.; Yoshimoto, M.; Tahara, K. Environmental impact of remanufacturing mining machinery. *Sustainability* **2022**, *14*, 8118. [CrossRef]
2.   Koide, R.; Murakami, S.; Nansaia, K. Prioritizing low-risk and high-potential circular economy strategies for decarbonization: A meta-analysis on consumer-oriented product-service systems. *Renew. Sustain. Energy Rev.* **2021**, *155*, 111858. [CrossRef]
3.   Seki, M.; Yoshida, A.; Ohue, Y.; Hongo, T.; Kawamura, T.; Shioyama, I. Influence of shot peening on surface durability of case-hardened steel gears. *J. Adv. Mech. Des. Syst. Manuf.* **2007**, *1*, 518–529. [CrossRef]
4.   Takahashi, K.; Amano, T.; Ando, K.; Takahashi, F. Improvement of fatigue limit by shot peening for high-strength steel containing a crack-like surface defect. *Int. J. Struct. Integr.* **2011**, *2*, 281–292. [CrossRef]
5.   Kubota, M.; Suzuki, T.; Hirakami, D.; Ushioda, K. Influence of hydrogen on fatigue property of suspension spring steel with artificial corrosion pit after multi-step shot peening. *ISIJ Int.* **2015**, *55*, 2667–2676. [CrossRef]
6.   Takahashi, K.; Kogishi, Y.; Shibuya, N.; Kumeno, F. Effects of laser peening on the fatigue strength and defect tolerance of aluminum alloy. *Fatigue Fract. Eng. Mater. Struct.* **2020**, *43*, 845–856. [CrossRef]
7.   Theresa, P.; Michael, H. Effect of laser peening on fatigue performance in 300M steel. *Fatigue Fract. Eng. Mater. Struct.* **2011**, *34*, 521–533.
8.   Sano, Y. Quarter Century Development oflaser peening without coating. *Metals* **2020**, *10*, 152. [CrossRef]
9.   Allan, H.C. Laser Shock Peening, the Path to Production. *Metals* **2019**, *9*, 626.
10. Soyama, H.; Alexander, M.K. A critical comparative review of cavitation peening and other surface peening methods. *J. Mater. Process. Tech.* **2022**, *305*, 117586. [CrossRef]
11. Takahashi, K.; Osedo, H.; Suzuki, T.; Fukuda, S. Fatigue strength improvement of an aluminum alloy with a crack-like surface defect using shot peening and cavitation peening. *Eng. Fract. Mech.* **2018**, *193*, 151–161. [CrossRef]
12. László, T. The poshibilities of the retained austenite reduction on tool steels. *Cryst. Eng.* **2021**, *6*, 99–105.
13. Yoshizaki, M. Improvement In Tooth Surface Strength Of Carburized Transmission Gears By Fine Particle Bombarding Carburized Process. In Proceedings of the 10th International Conference on Shot Peening, Tokyo, Japan, 15–18 September 2008.
14. Society of Automotive Engineers. *Residual Stress Measurement by X-ray Diffraction-SAE*; Society of Automotive Engineers: Warrendale, PA, USA, 1971; Volume J784a.
15. Tsuji, T.; Kobayashi, Y.; Inoue, K.; Ishikura, R. Influences of Mechanical Properties and Retained Austenite Content on Shot-peening Characteristics. In Proceedings of the 11th International Conference on Shot Peening, South Bend, IN, USA, 12–15 September 2011.
16. Hayama, M.; Kikuchi, S.; Komotori, J. Evaluation of the Compressive Residual Stress Relaxation Behavior by in situ X-ray Stress Measurement. *ISIJ Int.* **2022**, *62*, 758–765. [CrossRef]
17. Furuya, Y. Gigacycle fatigue of high-strength steel caused by MnS inclusions. *Mater. Sci. Eng. A* **2021**, *824*, 141840. [CrossRef]
18. Newman, J.C., Jr.; Raju, I.S. An Empirical Stress Intensity Factor Equation for the Surface Crack. *Eng. Fract. Mech.* **1981**, *15*, 185–192. [CrossRef]
19. American Petroleum Institute. *Recommended Practice 579, Fitness for Service*; American Petroleum Institute: Washington, DC, USA, 2000; pp. C3–C10.
20. Kitagawa, H.; Takahashi, S. Applicability of fracture mechanics to very small cracks or the crack in the early stage. In Proceedings of the Second International Conference on Mechanical Behaviour of Material, Boston, MA, USA, 16–20 August 1976.
21. El Haddad, M.; Topper, T.; Smith, N. Prediction of non propagating cracks. *Eng. Fract. Mech.* **1979**, *11*, 573–584. [CrossRef]
22. Ando, K.; Kim, M.H.; Nam, K.W. Analysis on peculiar fatigue fracture behaviour of shot peened metal using new threshold stress intensity factor range equation. *Fatigue Fract. Eng. Mater. Struct.* **2021**, *44*, 306–316. [CrossRef]